AIAA JOURNAL
Vol. 40, No. 5, May 2002

Compressive Response of Honeycombs Under In-Plane Uniaxial Static and Dynamic Loading, Part 2: Simulations

Jaeung Chung* and Anthony M. Waas†
University of Michigan, Ann Arbor, Michigan 48109-2140

The static and dynamic experimental results of polycarbonate circular cell honeycombs subjected to in-plane uniaxial loading are simulated through numerical analysis using the finite element method. The experimental results were presented in Part 1 (Chung, J., and Waas, A. M., "Compressive Response of Honeycombs Under In-Plane Uniaxial Static and Dynamic Loading, Part 1: Experiments," *AIAA Journal*, Vol. 40, No. 5, 2002, pp. 966–973). Through a comparison between the experimental results and numerical analysis, the crushing mechanism of the circular cell honeycomb material is studied. The influence of friction between the loading plate and the honeycomb material is studied numerically in the simulation of the dynamic experimental results.

I. Introduction

In Part 1 of this paper,[1] we observed and studied the compressive behavior of two-dimensional circular cell honeycombs made of polycarbonate subjected to two different in-plane loading conditions through an experiment. In the present paper, the corresponding numerical analysis via the commercial finite element code Abaqus is carried out statically and dynamically. The numerical analysis of the static experimental results is done by modeling the honeycomb material subjected to uniaxial loading in two different principal in-plane directions (X and Y directions), respectively. The numerical analysis of the dynamic experimental results is executed using the same circular cell honeycomb model as that used for the static simulation. Dynamic finite element analyses corresponding to the dynamic experiments of an initial impact velocity v_1 in each principal direction ($v_1 = 585$ mm/s in the X direction and $v_1 = 702$ mm/s in the Y direction) are carried out to check the experimental results numerically. The objective of the present study is to identify features of the compressive failure mechanism of these solids with the eventual goal of providing an understanding that will enable modeling of these materials as equivalent continua that reflect the observed experimental results. The latter is one of practical need because when cellular solids are used for large-scale structural applications, one has to resort to some degree of continuum modeling for the purpose of efficient numerical simulation. (There are several research investigations aimed at resolving the issue of how to characterize properly solids with microstructure as equivelent continua; see the work by Askar[2] and the references contained therein.) Once the initial identification stage is complete, the more important issue of predicting the energy absorbing characteristics of the honeycomb and a corresponding sandwich panel or sandwich structure can be accomplished satisfactorily. The present work has been carried out with these concerns in mind and is a preliminary step in the direction of attaining these larger goals.

Received 20 February 2001; revision received 2 October 2001; accepted for publication 8 October 2001.

*Research Fellow, Department of Aerospace Engineering; chungae@engin.umich.edu.

†Professor, Department of Aerospace Engineering; dcw@engin.umich.edu. Associate Fellow AIAA.

II. Static Case

A. Numerical Procedure

The static response of the honeycomb was studied via the finite element method. The commercial code Abaqus (the implicit version) was used for this purpose. In the finite element analysis (FEA), a model was made of the entire microsection of the honeycomb (Fig. 2b in Ref. 1) using averaged measured representative data as recorded via an optical microscope. The model includes wall thickness variations and cell ellipticity (Fig. 3 in Ref. 1). The procedure to generate the FEA mesh for the 12×12 cell microsection was as follows: Cell wall thickness variation and cell ellipticity of the microsection of the honeycomb was painstakingly measured for several 12×12 cell specimens. The data were gathered and analyzed to obtain average cell ellipticity, average cell wall thickness variation, average double wall thickness (occurring at those locations where two cells meet), and average contact area. Next, a microsection of the honeycomb was meshed that included these average measured properties. After this, the microsection was periodically extended in the horizontal and vertical directions to generate the entire 12×12 cell model of the test specimen. Thus, the 12×12 FEA mesh is periodic, with the microsection representing the average values of geometrical imperfections and cell ellipticity as recorded through the measurements carried out via an optical microscope. In the first step of the analysis, a linear elastic eigenvalue analysis is carried out to obtain the eigenmode shapes of the 12×12 cell model. The eigenmode shape corresponding to the lowest eigenvalue is used to perturb the mesh. In addition, the 12×12 cell model is artificially perturbed at the location of the severest localization as observed in the experiment. The magnitude of this perturbation is such that the resulting linear slope of the numerical response is unaffected. That is, beyond a certain size of the magnitude, the linear slope shows a strong dependence on the magnitude. In the present work, the largest possible magnitude that shows no change in the resulting slope of the linear response was used. The largest possible magnitude was determined through several simulations having several different magnitudes of perturbation, respectively.

The microsection of the honeycomb is discretized with three-noded quadratic beam elements. The beam element (B22) is based on Timoshenko beam theory and includes transverse shear deformation. The transverse shear deformation in this element is treated as if the response were linear elastic, independent of the axial and bending responses. This feature is used to analyze nonlinear geometric and nonlinear material behavior. Each cell of the honeycomb is modeled with 20 curved beam elements, and the contact region between neighboring cells is made of 2 beam elements. To include thickness variation, each beam element in the microsection of the honeycomb has a different thickness that is representative of what was measured through the optical microscope (Fig. 4 in Ref. 1). To prevent penetration among cells during deformation, contact elements

were included. When rigid bar elements are used to simulate the loading plates, the model is subjected to displacement-controlled loading along the X direction and along the Y direction, respectively. In addition, contact elements between the rigid bars and the honeycomb materials are used to prevent penetration. The honeycomb material is initially elastic and then exhibits plasticlike behavior. It is well known that polymeric materials such as polycarbonate exhibit yieldlike phenomena found in metals, although the mechanism by which a metal exhibits plasticity is quite different from that of a polymer. Nevertheless, for the purposes of simulation, it is convenient and appropriate to resort to classical $J2$ (volume preserving) small strain incremental theory of plasticity for modeling the constitutive behavior of the honeycomb material. The basic elements of this theory are well documented in several texts (for example, that by Lubliner[3]). In the Abaqus commercial code, this theory is provided via a builtin routine that needs as its input the complete uniaxial stress–strain response of the material (Fig. 2a in Ref. 1). In Fig. 2a in Ref. 1, the stress and strain are true stress and logarithmic strain, respectively. With individual data points provided on this curve manipulated according to what is required by Abaqus, the material specification that conforms to $J2$ incremental theory of plasticity is completed. Details of the theory are ommitted here for the sake of brevity and may be found in Ref. 3 and other plasticity texts, such as that by Mendelson.[4]

B. Static Compressive Loading in X Direction

The experimental and numerical responses of a honeycomb specimen under a compressive loading in the X direction are shown in Fig. 1a. Figure 1b and Fig. 6b in Ref. 1 show a sequence of deformed configurations of the specimen in the simulation and the experiment, respectively. In Fig. 1a, the straight line is the macroscopic stress in the X direction to the macroscopic strain in the X direction response as measured in the experiment and the dashed line is the response as obtained via the simulation. The circles and triangles in Fig. 1a indicate the locations of the experimental and numerical responses related to the deformed configurations of the specimen in the experiment and the simulation, respectively. Initially, the model deforms in a uniform fashion (Fig. 1b, sxs1). The slope of the numerical response begins to change due to a reduction in the stiffness of the specimen caused by initiation of localization (Fig. 1b, sxs2 and sxs3). Then, the numerical response experiences stable nonlinearity until the response reaches a maximum stress (Fig. 1b, sxs4). Development of severe localization such as X-band shape at the left part of the specimen causes the numerical response to exhibit unstable nonlinear behavior. After this, cell wall contact causes the slope of the response to change from negative to positive (Fig. 1b, sxs5 and sxs6). Severe localization is found to occur along the diagonals of the specimen (more to the left part of the specimen, as shown in Fig. 1b, sxs6). Localization into an X-band shape was found in the right part of the specimen in the experiment. As seen in Fig. 1a, the numerical response shows good agreement with the experimental response. The predicted difference in the maximum load in both cases is within 6% of the measured maximum load. Clearly, these differences are to be expected because the numerical model includes the microsection of the honeycomb with average geometric properties, which is periodically extended to form the 12×12 simulation model. This is quite different from the variations that are present in a particular test specimen.

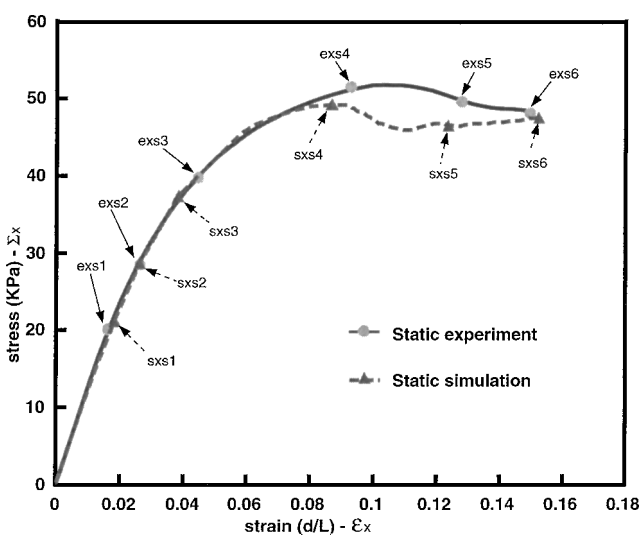

Fig. 1a Static stress–strain response under compressive loading in X direction.

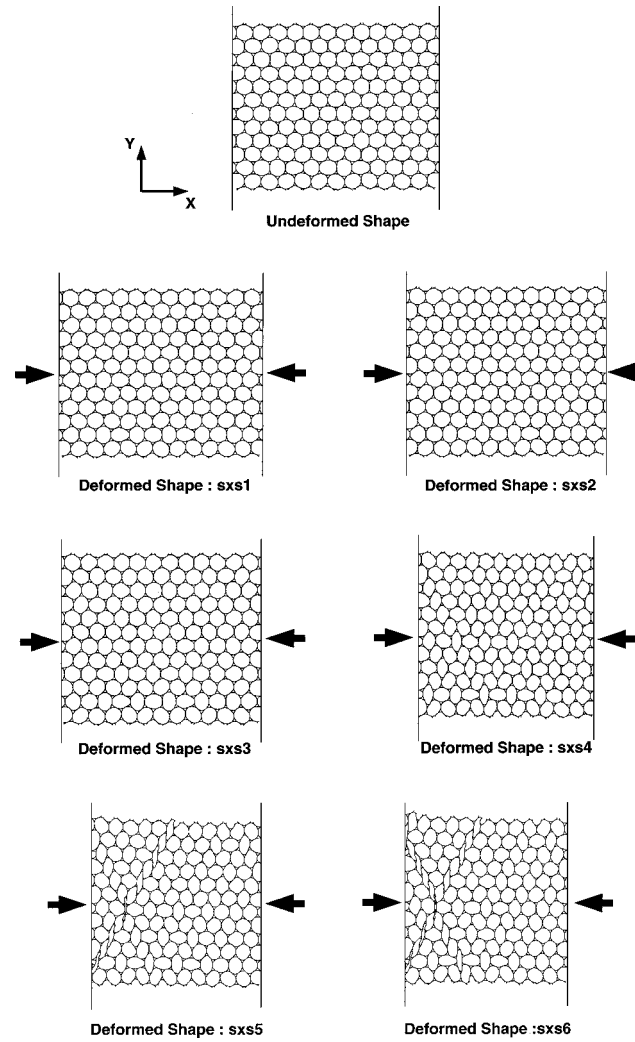

Fig. 1b FEA simulation: sequence of deformed honeycomb specimen under static compressive loading in X direction.

C. Static Compressive Loading in Y Direction

The experimental and numerical responses of a honeycomb specimen under a compressive loading in the Y direction are shown in Fig. 2a. Figure 7b in Ref. 1 shows a sequence of deformed configurations of the specimen in the experiment and Fig. 2b (here) shows the corresponding sequence in the simulation. In Fig. 2a, the stright line is the macroscopic stress in the Y direction to macroscopic strain in the Y direction response in the experiment, and the dashed line is the response as predicted via the simulation. The finite element model of the circular cell honeycomb experiences linear deformation initially (Fig. 2b, sys1), and then stable nonlinear behavior occurs in the model (Fig. 2b, sys2 and sys3) until the maximum stress is reached (Fig. 2b, sys4). Beyond the maximum stress, the response is unstable and nonlinear (Fig. 2b, sys5 and sys6) until the cell walls of the honeycomb material contact each other. When the cell walls contact each other, the slope of the numerical response becomes positive for a while (Fig. 2b, sys7–sys9), and then the slope changes from positive to negative again due to collapse of other cells, until cell walls contact begins again. The second row

from the bottom of the specimen was significantly more localized when compared to other localized rows (Fig. 2b, sys5), whereas, in the experiment, the third row was deformed most significantly among the rows of the specimen (Fig. 7b, eys5, in Ref. 1). As seen in Fig. 2a, the predicted stiffness of the response in the linear region matched the experimental result very well. The difference between the maximum loads corresponding to the two cases is about 15% of the experimental value.

III. Dynamic Case

A. Numerical Procedure

The experimentally measured dynamic response of the honeycomb was studied through the finite element method. In the dynamic FEA (DFEA), the geometric model adopted in the static numerical simulation is used. In other words, the numerical model of the honeycomb material is made by periodic extension of the microsection of the test specimen measured directly through an optical microscope. The only difference between the static and dynamic model is the location in the numerical model of the perturbation associated with the first eigenmode shape. That is, the numerical model is perturbed more at the location of the severest localization in the honeycomb specimen observed in the dynamic experiment. Like in the static numerical model, each cell of the honeycomb is discretized with a three-noded beam element (B22), and contact elements are used to prevent penetration among cells during deformation in the dynamic numerical model. To simulate the loading plates, rigid bar elements are used. In addition, contact elements between the rigid bars and the honeycomb are used to prevent penetration. To specify the plastic part of the polycarbonate honeycomb material, small strain J2 incremental theory of plasticity is used.[3,4] To model the viscoplastic character of the honeycomb material in the DFEA, the RATE DEPENDENT option provided in Abaqus is used. This assumes that the material obeys a power law relation between the plastic strain rate and the rate dependent yield stress. Thus, for $\bar{\sigma} \geq \sigma^0$,

$$\dot{\bar{\varepsilon}}^{\mathrm{pl}} = D[(\bar{\sigma}/\sigma^0) - 1]^p$$

where

D, p = material parameters
$\dot{\bar{\varepsilon}}^{\mathrm{pl}}$ = equivalent plastic strain rate
$\bar{\sigma}$ = yield stress at the nonzero plastic strain rate
σ^0 = static yield stress

In the equation, D and p are determined from Fig. 2a in Ref. 1. The numerical analysis enforces the same physical boundary conditions as that in the dynamic experiment by enforcing the measured time vs displacement data obtained through the experiment in the DFEA.

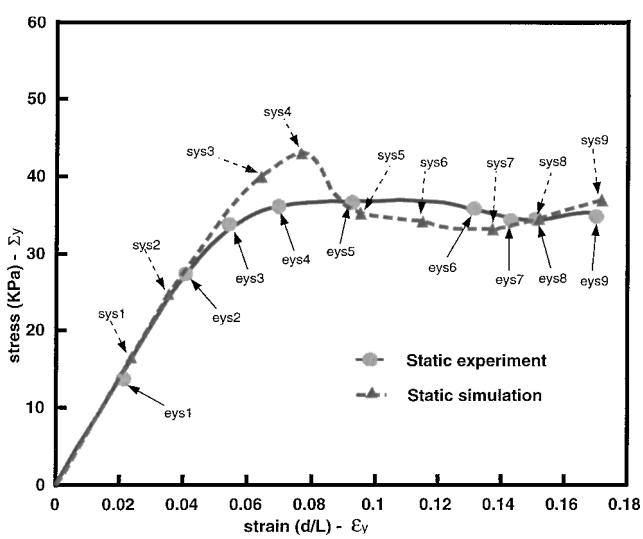

Fig. 2a Static stress–strain response under compressive loading in *Y* direction.

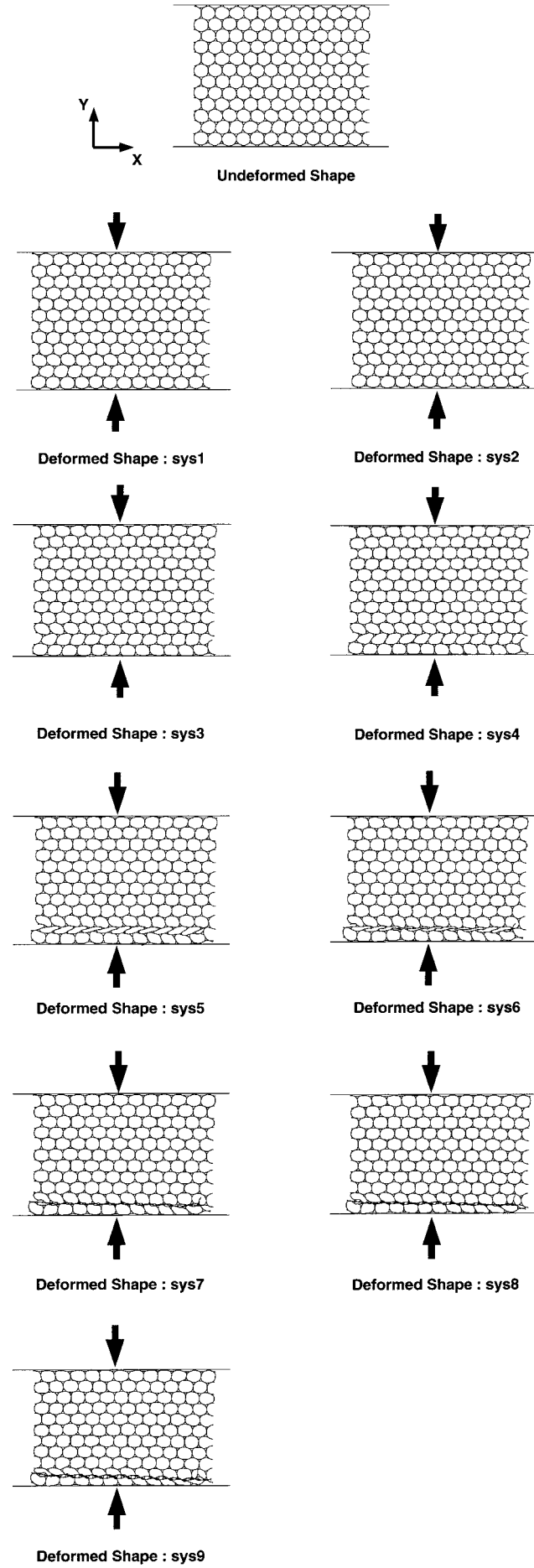

Fig. 2b FEA simulation: sequence of deformed honeycomb specimen under static compressive loading in *Y* direction.

That is, displacement boundary loading as a function of time is enforced.

In the dynamic experiments, the test specimen is attached to the lower steel block using an epoxy adhesive to prevent the test specimen from moving from its original location. To enforce this experimental constraint in the numerical model, in the dynamic numerical analysis corresponding to an X direction impact loading, the left side nodes of the model contacting the rigid bar element (Fig. 3b, undeformed shape) are fixed. In the dynamic numerical analysis corresponding to a Y direction impact loading, the bottom nodes of the model connected to the lower rigid bar (Fig. 4b, undeformed shape) are fixed.

In the dynamic experiments, when the free falling upper loading plate impacts the specimen, friction occurs between the specimen and the loading plate (see Figs. 10b and 11b in Ref. 1). As seen in Figs. 10b and 11b in Ref. 1, friction effects between the specimen and the loading plate under the X direction impact loading are larger than the friction effects between the specimen and the loading plate under the Y direction impact loading. Hence, in the dynamic simulation under X direction impact loading, the right side nodes of the numerical model (Fig. 3b, undeformed shape) contacting the right rigid bar are not allowed to move in the Y direction. In the dynamic simulation under the Y direction impact loading, the top side nodes of the numerical model (Fig. 4b, undeformed shape) contacting the upper rigid bar are free to move in the X direction. In the discussion that follows, the effect of friction between the impactor and the specimen will be discussed through a comparison of three cases for each in-plane loading direction ($\mu = 0$, $\mu = 0.05$, and fixed case, where μ is the coefficient of friction between the two surfaces).

B. Dynamic Compressive Loading in X Direction

The experimental and numerical responses of a honeycomb specimen under an impact compressive loading with an initial impact velocity of 585 mm/s in the X direction are shown in Fig. 3a. Figure 10b in Ref. 1 and Fig. 3b (here) show a sequence of deformed configurations of the specimen in the experiment and simulation, respectively. In Fig. 3a, the straight line is the macroscopic stress in the X direction to the macroscopic strain in the X direction response in the experiment, and the dashed line is the numerical response. Squares and triangles on the response curves in Fig. 3a indicate the stress and strain values corresponding to the mode shapes in the experimental and numerical responses, respectively. In Fig. 3a, the experimental and numerical responses are shown up to the maximum displacement of the specimen during the impact event. In the first phase of the numerical response, the finite element model of the honeycomb material deforms symmetrically about the loading direction (Fig. 3b, sxd1). Next, the model experiences stable nonlinearity (Fig. 3b, sxd2 and sxd3) caused by the initiation of localization until the maximum stress is reached (Fig. 3b, sxd4). After the maximum stress, the slope of the numerical response changes to negative (Fig. 3b, sxd5) until some cell walls of the model contact each other (Fig. 3b, sxd6). As seen in Fig. 3b, sxd4–sxd6, the localized band in the simulation is formed along a diagonal line from the fourth cell (from the left end of the top row) to the third cell (from the right end of the bottom row) and an adjacent diagonal line on the right side of this line. This localized band is similar to that found in the experiment. The development of this localized band causes the slopes of the experimental and numerical responses to change from positive to negative.

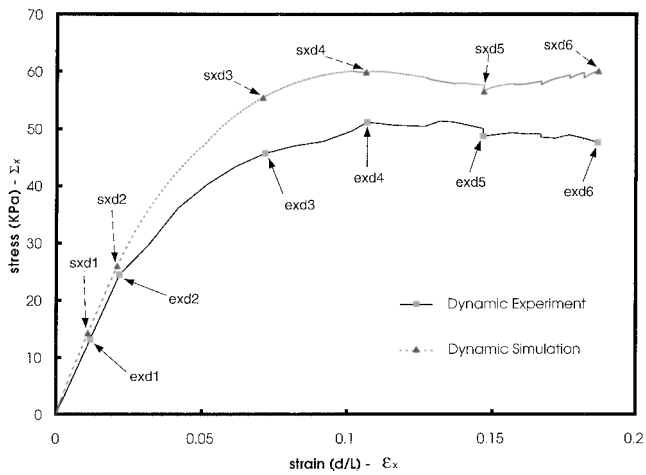

Fig. 3a Dynamic stress–strain response under impact compressive loading with initial impact velocity of 585 mm/s in X direction.

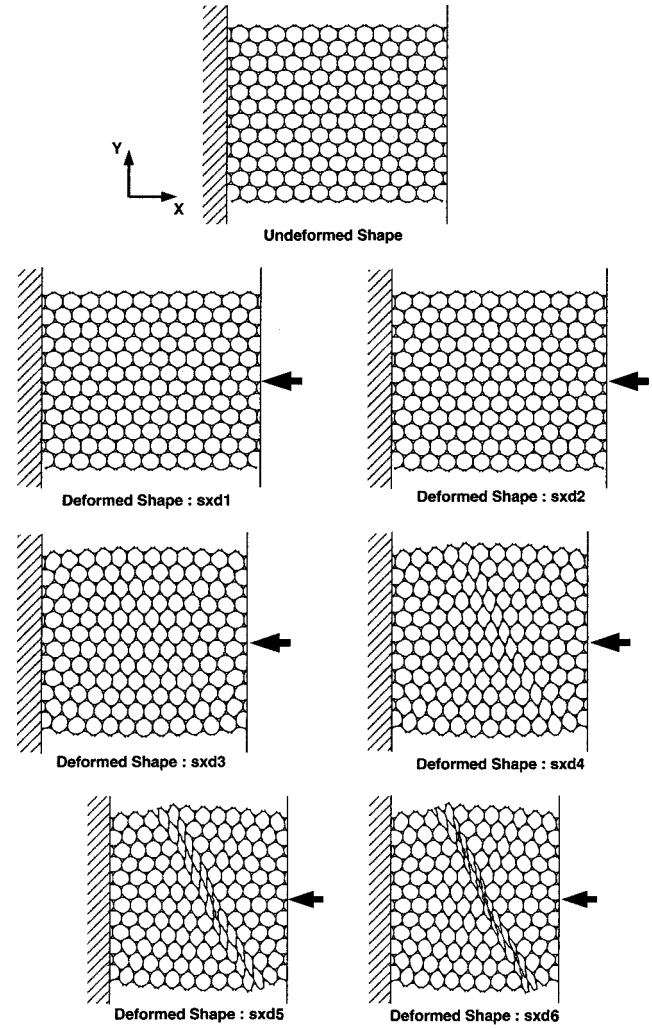

Fig. 3b FEA simulation: sequence of deformed honeycomb specimen under impact compressive loading with the initial impact velocity of 585 mm/s in X direction.

C. Dynamic Compressive Loading in Y Direction

The experimental and numerical responses of a honeycomb specimen under an impact compressive loading with an initial impact velocity of 702 mm/s in the Y direction are shown in Fig. 4a. Figure 4b shows a sequence of deformed configurations of the specimen through simulation and the corresponding sequence of deformed configurations in the experiment is shown in Fig. 11b in Ref. 1. In Fig. 4a (here), the straight line is the macroscopic stress in the Y direction to the macroscopic strain in the Y direction response in the experiment, and the dashed line is the numerical response. Squares and triangles on the response curves in Fig. 4a indicate the values of stress and strain corresponding to the mode shapes in the experimental and numerical responses, respectively. In Fig. 4a, the experimental and numerical responses are shown up to the maximum displacement of the specimen caused by the initial loading condition. The numerical model of the honeycomb material exhibits an initial linear response (Fig. 4b, syd1). This progresses to a nonlinear but stable behavior (Fig. 4b, syd2 and syd3) until the maximum stress is reached. As seen in Fig. 4b, syd2, the third and fourth rows (from the bottom row) are localized into a zigzag shape. As seen

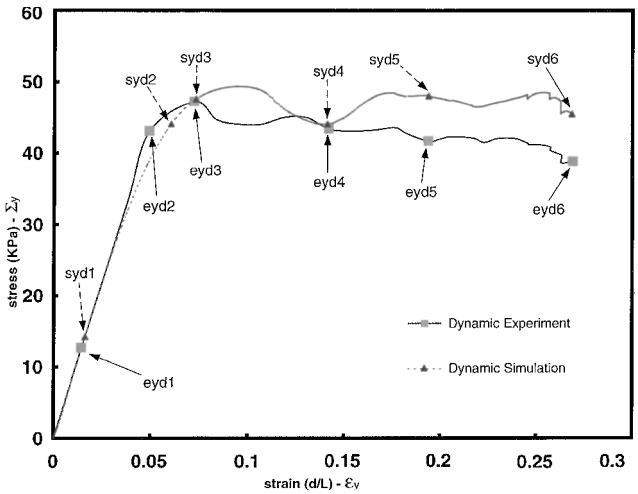

Fig. 4a Dynamic stress–strain response under impact compressive loading with the initial impact velocity of 702 mm/s in *Y* direction.

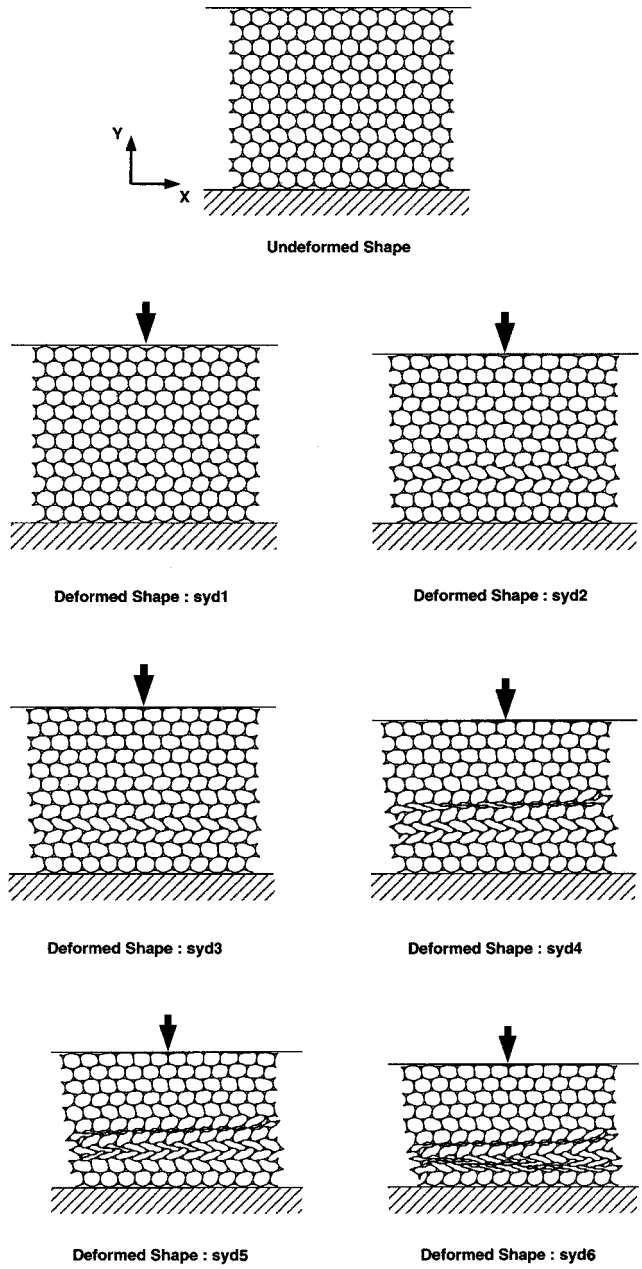

Fig. 4b FEA simulation: sequence of deformed honeycomb specimen under impact compressive loading with the initial impact velocity of 702 mm/s in *Y* direction.

in Fig. 4b, syd4, the cell walls of the sixth row (from the bottom row) are totally in contact with each other and the left side cells of the third and fourth rows have deformed more severely than the other cells of these rows. Beyond the state corresponding to Fig. 4b, syd4, of the numerical response, the slope of the response starts to change from negative to positive. The slope of the numerical response corresponding to the deformed shapes between Fig. 4b, syd5, and Fig. 4b, syd6, changes from negative to positive and back to negative again. This variation of the response is caused by some cell walls of the third and fourth rows contacting each other. Deformed configurations in the simulation are identical to these found in the experiment. The difference between mode shapes observed in the experiment and the numerical simulation is the cause of the difference in the macroscopic stress and strain between the experimental and numerical response. However, the difference between the two responses is not so large. The numerical response still predicts the experimental response resonably well and captures the trends of the experimental response.

IV. Discussion

From the experimental and numerical results, the linear stiffnesses of the static and dynamic response in the *X* direction is higher than those in the *Y* direction. This is mainly caused by deviation from circularity for each cell of the specimen. In other words, if each cell of the specimen is perfectly circular, the linear stiffnesses in the *X* and *Y* directions are equal. If each cell is elliptic, then the linear stiffnesses are dependent on the cell aspect ratio.

Hence,

$$E_x^* = E_y^* \quad \text{if} \quad a = b$$

$$E_x^* > E_y^* \quad \text{if} \quad a > b$$

$$E_x^* < E_y^* \quad \text{if} \quad a < b$$

where

a = diameter of an elliptical cell in the X direction
b = diameter of an elliptical cell in the Y direction

The preceding results on elastic stiffness have been derived and explained in detail in Ref. 5. In Tables 1 and 2, the linear stiffnesses of the full-scale numerical simulation are compared to experimentally measured linear stiffnesses of the honeycombs statically and dynamically. Because the full-scale numerical model has imperfections, such as cell size, wall thickness, wall thickness variation, and deviation from circularity for each cell, the numerical analysis using the model shows good agreement with the experimental results.

The macroscopic orthotropy in elastic stiffness due to the discussed imperfections acts synergistically with orthotropy induced due to deformation, resulting in the observed and predicted localized deformation patterns in the postbuckled regime of the specimen response. Indeed, the *X*-direction response and proceeding diagonal localized deformation bands are in stark contrast to

Table 1 Comparison of static linear stiffnesses for full-scale numerical simulations and experimental results

Static loading	12 × 12 cell section including imperfections, numerical	12 × 12 cell section, experiment
E_x^*, kPa	1178	1176
E_y^*, kPa	699	693

Table 2 Comparison of linear stiffnesses for full-scale dynamic numerical simulations and dynamic experimental results with initial impact velocity v_1

Dynamic loading	12 × 12 cell section including imperfections, numerical	12 × 12 cell section, experiment
E_x^*,[a] kPa	1289	1128
E_y^*,[b] kPa	882	875

[a]Velocity $v_1 = 585$ mm/s. [b]Velocity $v_1 = 702$ mm/s.

the Y-direction response and the corresponding parallel localized deformation bands. Thus, if we were to model these honeycombs as equivalent continua, then a representation that involves macroscopic orthotropy (because of initial imperfections and that which is induced by deformation) is essential to capture properly the observed localized deformation patterns. What we have here is initial geometric imperfections and cell deformation at the microscopic level, resulting in an effect at the macroscopic level that is reflected via the equivalent (macroscopic) constitutive description of the solid, which essentially renders the solid to be orthotropic. As seen in Figs. 1a and 2a, the discrepancy between the experimental response and the numerical prediction for the Y-direction static loading, in the nonlinear regime, is larger than the corresponding discrepancy between the reponses under X-direction static loading (in the nonlinear regime). This is caused by the degree of relative accuracy of the imperfection in the numerical model. In other words, if the imperfection is more accurately prescribed in the numerical model, that is, the numerical model is closer in geometry to the real test specimen, the numerical response becomes closer to the experimental response. As seen in Figs. 1b, Fig. 6b in Ref. 1, Fig. 2b, and Fig. 7b in Ref. 1, the deformed numerical model under X-direction static loading is closer to the deformed test specimen in comparison with the deformed model and test specimen under Y-direction static loading. The experimental results (Figs. 1a, 2a, 3a, and 4a) indicate another feature that is related to the observed orthotropy of the honeycomb specimens. In the static experiments, the maximum macroscopic stress in the X direction, Σ_x, is approximately 52 kPa, whereas the corresponding maximum macroscopic stress in the Y direction, Σ_y, is 37 kPa (Table 3). In the dynamic experiments with an initial impact velocity v_1, the maximum macrscopic stress in the X direction, Σ_x^d, is around 51 kPa ($v_1 = 585$ mm/s) and the maximum macroscopic stress in the Y direction, Σ_y^d, is around 47 kPa ($v_1 = 702$ mm/s) (Tables 4 and 5). These numbers were predicted with reasonable accuracy via the full-scale numerical simulations reported herein (Tables 3–5). As seen in Tables 3–5, Young's moduli of the dynamic numerical responses are higher than those of the static numerical responses in both principal in-plane directions. This is caused by the following reasons. First, the linear slope of the response simulated dynamically is usually higher than that of the statically simulated response because the inertia of the impacting mass drives the material response to be time dependent, with a higher linear stiffness as the strain rate increases. Second, the nodes located on the left-end X-direction loading case (correspondingly, the bottom for the Y-direction loading case) of the dynamic numerical model are fixed on the rigid bar, and the nodes located on the right-end X-direction loading case (correspondingly, the top for the Y-direction loading case) of the model are affected by friction, whereas the nodes at the left end (the bottom) and the right end (the top) of the static numerical model is free to move on the loading rigid bars. These stiffer boundary conditions in the dynamic numerical model compared to those in the static model also contribute to making the linear slope of the response to be higher in the dynamic case. The dynamic numerical responses with friction included between the rigid bar (impactor) and the nodes of the right-end X-direction loading case (the top nodes for the Y-direction loading case) are compared with the dynamic experimental responses in Figs. 5 and 6 and Tables 6 and 7. In Figs. 5 and 6, we show results for three different cases: the first with $\mu = 0$, the second with $\mu = 0.05$, and finally a fully fixed (clamped) case. As seen in Figs. 5 and 6, as the friction force increases, Young's modulus and maximum stress tend to increase. The friction condition does not affect Young's modulus of the dynamic numerical response in the X direction when compared to that in the Y direction. In other words, the linear response of the numerical model in the Y direction reacts to the friction condition (occuring between the impactor and the honeycomb model) more

Table 3 Comparison of maximum stress vs corresponding strain in static experimental results and numerical simulation

	Maximum stress, kPa/strain, %	
Direction	Experiment	Simulation
X	52/10.3	49/8.6
Y	37/10	43/7.7

Table 4 Comparison of maximum stress vs corresponding strain and maximum strain vs corresponding stress in dynamic experimental results and numerical simulation with initial impact velocity $v_1 = 585$ mm/s in X direction

Method	Maximum stress, kPa/strain, %	Maximum strain, %/stress, kPa
Experiment	51/10.7	18.7/48
Simulation	60/10.6	18.7/60

Table 5 Comparison of maximum stress vs corresponding strain and maximum strain vs corresponding stress in the dynamic experimental results and numerical simulation with initial impact velocity $v_1 = 702$ mm/s in Y direction

Method	Maximum stress, kPa/strain, %	Maximum strain, %/stress, kPa
Experiment	47/7.2	26.9/39
Simulation	49/9.5	26.9/45

Table 6 Dynamic uniaxial experiment compared with dynamic numerical simulations, $v_1 = 585$ mm/s, X direction

Method	Young's modulus, kPa	Maximum stress, kPa/strain, %	Maximum strain, %/stress, kPa
Experiment	1128	51/10.7	18.7/48
Simulation ($\mu = 0$)	1226	59/14.4	18.7/54
Simulation ($\mu = 0.05$)	1238	59/15.4	18.7/58
Simulation (fixed)	1289	60/10.6	18.7/60

Table 7 Dynamic uniaxial experiment compared with dynamic numerical simulations, $v_1 = 702$ mm/s, Y direction

Method	Young's modulus, kPa	Maximum stress, kPa/strain, %	Maximum strain, %/stress, kPa
Experiment	875	47/7.2	26.9/39
Simulation ($\mu = 0$)	882	49/9.5	26.9/45
Simulation ($\mu = 0.05$)	912	51/9.4	26.9/48
Simulation (fixed)	1120	51/8.1	26.9/46

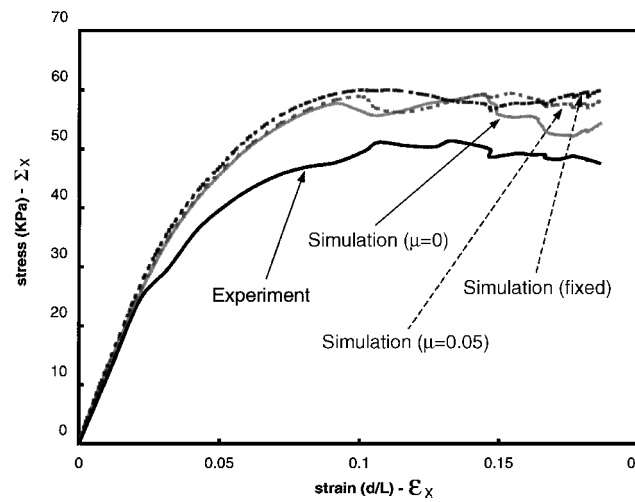

Fig. 5 Effect of friction between the impactor and the honeycomb specimen through comparison of dynamic uniaxial experiment and three dynamic numerical simulations with the initial impact velocity $v_1 = 585$ mm/s in X direction.

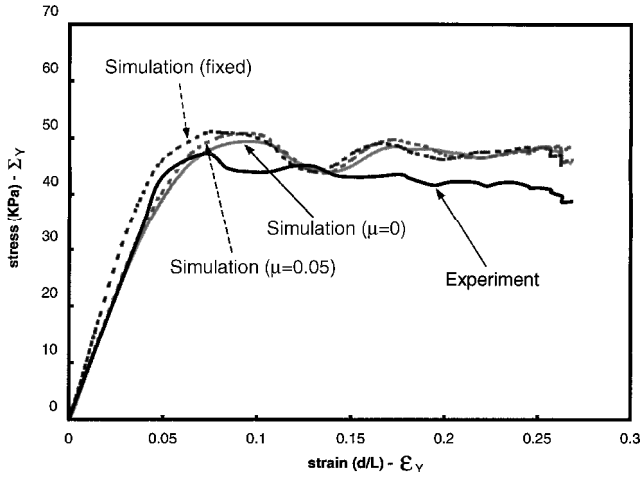

Fig. 6 Effect of friction between the impactor and the honeycomb specimen through comparison of dynamic uniaxial experiment and three dynamic numerical simulations with the initial impact velocity v_1 = 702 mm/s in *Y* direction.

sensitively than that in the *X* direction. Note that these static and dynamic simulations include the static and dynamic plastic behavior of the polycarbonate material, which has a significant influence on the maximum (plateau) stress carrying capability of the honeycomb, respectively. This latter aspect is important in predicting the energy absorbing capability of the honeycomb.[6] The biaxial characterization, reported by Chung,[7] is needed to clearly ascertain the energy absorbing characteristics of these honeycombs under more general multiaxial loading situations.

V. Conclusions

The results from a combined experimental and analytical study on the crushing response of circular celled polycarbonate honeycombs under uniaxial compressive loading in two mutually orthogonal directions were reported by Chung and Waas[1] and were numerically simulated via the finite element method in this paper. Our results show that hexagonally packed nominally circular cell honeycombs are orthotropic (not transversely isotropic as would be expected in the perfect case). Initial cell ellipticity, nonuniform contact between neighboring cells, and deformation-induced orthotropy (because of the manner in which the cells are packed) are found to be major causes of this deviation from intended behavior. This macroscopic orthotropy is reflected in various aspects of the crushing response. For example, the linear stiffness, the localized deformation mode, and the maximum (plateau) stress are all affected. Equivalent macroscopic characterizations of such honeycombs must reflect these observed experimental findings because they bear heavily on our ability to predict accurately the energy absorbing characteristics of these honeycomb core materials and corresponding sandwich panels made with these materials.

References

[1]Chung, J., and Waas, A. M., "Compressive Response of Honeycombs Under In-Plane Uniaxial Static and Dynamic Loading, Part 1: Experiments," *AIAA Journal*, Vol. 40, No. 5, 2002, pp. 966–973.

[2]Askar, A., *Lattice Dynamical Foundations of Continuum Theories*, World Scientific, Singapore, 1943, Chap. 4.

[3]Lubliner, J., *Plasticity Theory*, Macmillan, New York, 1990, Chap. 3.

[4]Mendelson, A., *Plasticity: Theory and Application*, Krieger, Malabar, FL, 1986, Chap. 7.

[5]Chung, J., and Waas, A. M., "The Inplane Elastic Properties of Circular Cell and Elliptic Cell Honeycombs," *Acta Mechanica*, Vol. 144, No. 1–2, 2000, pp. 29–42.

[6]Gibson, L. J., and Ashby, M. F., *Cellular Solids: Structure and Properties*, 2nd ed., Cambridge Univ. Press, Cambridge, England, U.K., 1997, Chap. 8.

[7]Chung, J., "Inplane Compressive Response and Failure of Circular Cell Honeycomb," Ph.D. Dissertation, Dept. of Aerospace Engineering, Univ. of Michigan, Ann Arbor, MI, 2000, Chaps. 4, 5.

S. Saigal
Associate Editor